



#### **PAPER • OPEN ACCESS**

# CO<sub>2</sub> snow jet cleaning as a roll-to-roll compatible method for deburring IMI substrates after laser patterning

To cite this article: M Wagner et al 2023 Flex. Print. Electron. 8 015007

View the article online for updates and enhancements.

#### You may also like

- Burr removal from high-aspect-ratio micropillars using ultrasonic-assisted abrasive micro-deburring

A Sravan Kumar, Sankha Deb and S Paul

- Surface quality improvement of milled Aluminum-6061 using magnetic abrasive deburring

M A Rahma, A Satrial, K Saptaji et al.

- Mathematical modeling and hydrodynamics of Electrochemical deburring process

Satisha Prabhu and K Abhishek Kumar

#### Flexible and Printed Electronics



#### **OPEN ACCESS**

#### RECEIVED

10 October 2022

#### REVISED

26 December 2022

ACCEPTED FOR PUBLICATION
6 January 2023

#### PUBLISHED

31 January 2023

Original content from this work may be used under the terms of the Creative Commons Attribution 4.0 licence.

Any further distribution of this work must maintain attribution to the author(s) and the title of the work, journal citation and DOI.



#### **PAPER**

## CO<sub>2</sub> snow jet cleaning as a roll-to-roll compatible method for deburring IMI substrates after laser patterning

M Wagner<sup>1,2</sup>, A Distler<sup>1</sup>, H-DHD Schmidt<sup>1</sup>, A Classen<sup>3</sup>, T Stubhan<sup>3</sup>, M Koegl<sup>3</sup>, J Illg<sup>4</sup>, C J Brabec<sup>1,2</sup> and H-JHJ Egelhaaf<sup>1,2,\*</sup>

- <sup>1</sup> Friedrich-Alexander University Erlangen-Nürnberg, Institute of Materials for Electronics and Energy Technology, Solar Factory of the Future, Fürther Str. 250, 90429 Nürnberg, Germany
- Helmholtz Institute Erlangen-Nürnberg (HI-ERN), Immerwahrstr. 2, 91058 Erlangen, Germany
- <sup>3</sup> SCIPRIOS GmbH, Fürther Str. 244a, 90429 Nürnberg, Germany
- <sup>4</sup> acp systems AG, Berblingerstr. 8, 71254 Ditzingen, Germany
- \* Author to whom any correspondence should be addressed.

E-mail: hans-joachim.egelhaaf@fau.de

**Keywords:** transparent electrode, laser patterning, deburring, carbon dioxide snow jet, printed photovoltaics Supplementary material for this article is available online

#### Abstract

Burring is commonly encountered upon patterning of dielectric-metal-dielectric (DMD) transparent electrodes by laser ablation. These burrs are conductive and thus lead to shunting of the (opto-)electronic devices built upon these electrodes. In this work, CO<sub>2</sub> snow jet blasting is presented as a convenient and reliable method for deburring laser-patterned DMD electrodes during roll-to-roll manufacturing of organic solar modules. As CO<sub>2</sub> snow jet blasting significantly reduces the extent of shunting and concomitantly avoids scratching the electrode, the photoelectrical conversion efficiencies of the solar modules thus produced are higher than those obtained for traditional deburring techniques.

#### 1. Introduction

Printed electronics has recently received a boost in all application areas, such as light emitting diodes, field effect transistors, photovoltaics, as well as photoand x-ray detectors, due to the development of new, efficient materials. This is especially true for printed photovoltaics. On the one hand, perovskite solar cells have reached certified efficiencies of up to 25.7%, within only a few years after their discovery, but also organic photovoltaics (OPV) has experienced an impressing increase in efficiency over the recent years, due to the advent of non-fullerene acceptors, which have enabled certified record efficiencies of 18.2% on small area devices [1], with a few reports even claiming efficiencies very close to the 20% threshold (19.6%) [2]. Also with respect to lifetime, impressing values have been reported recently for both technologies [3].

Printed Photovoltaics (PV) having thus reached the maturity for commercialization, upscaling of the technology poses new challenges, e.g. in terms of transferring the record efficiencies achieved with small laboratory cells of less than 1 cm<sup>2</sup> area to largearea modules, but also with respect to low-cost high throughput production. Recent advances in both, OPV and perovskite technologies have reduced efficiency losses upon upscaling significantly, with efficiencies of 23.7% being reported for a 1 cm<sup>2</sup> perovskite solar cell and 17.9% for an 800 cm<sup>2</sup> solar module [4, 5]. In OPV technology, an efficiency of 15.2% has been achieved for a 1 cm<sup>2</sup> solar cell and a record efficiency of 11.7% has been reported for a 200 cm<sup>2</sup> solar module [4, 6].

Printed PV is ideally suited for low-cost production, as it can be manufactured by low-temperature, high-throughput roll-to-roll (R2R) processes. Both, in perovskite and organic PV, high quality R2R production has been demonstrated recently [7–9]. In R2R production, the monolithic interconnection of the individual cells (which are typically 5–10 mm in width) [10] to form the module is realized mostly by short-pulse laser ablation [11–14], as this is the most convenient way to achieve sufficiently narrow interconnection zones (down to 100  $\mu$ m) [10] to reach geometric fill factors (FFs) exceeding 95%.

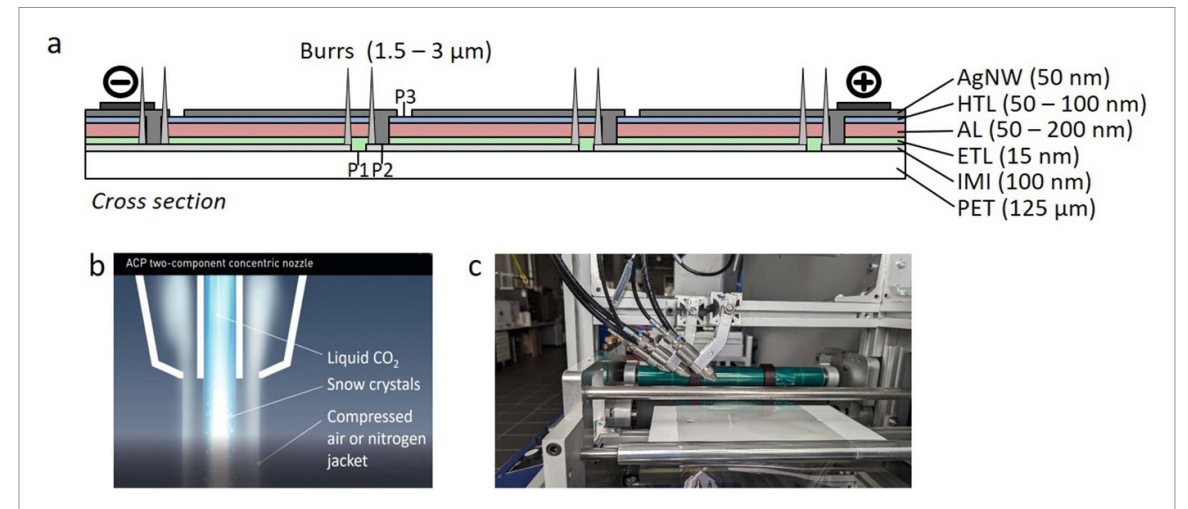


**Figure 1.** (a): Stack of the individual layers of a printed solar cell (ETL—electron transport layer, AL—active layer, HTL—hole transport layer, AgNW—silver nanowire electrode. P1, P2, P3—laser lines in IMI electrode, AL, and top electrode, respectively, for electrical interconnection of the individual cells). Note that the thickness of the layer stack ETL/active layer/HTL is significantly less than 1  $\mu$ m. (b): schematic view of a concentric CO<sub>2</sub> snow jet. (c): CO<sub>2</sub> snow jet array installation on the machine for roll-to-roll PV manufacturing.

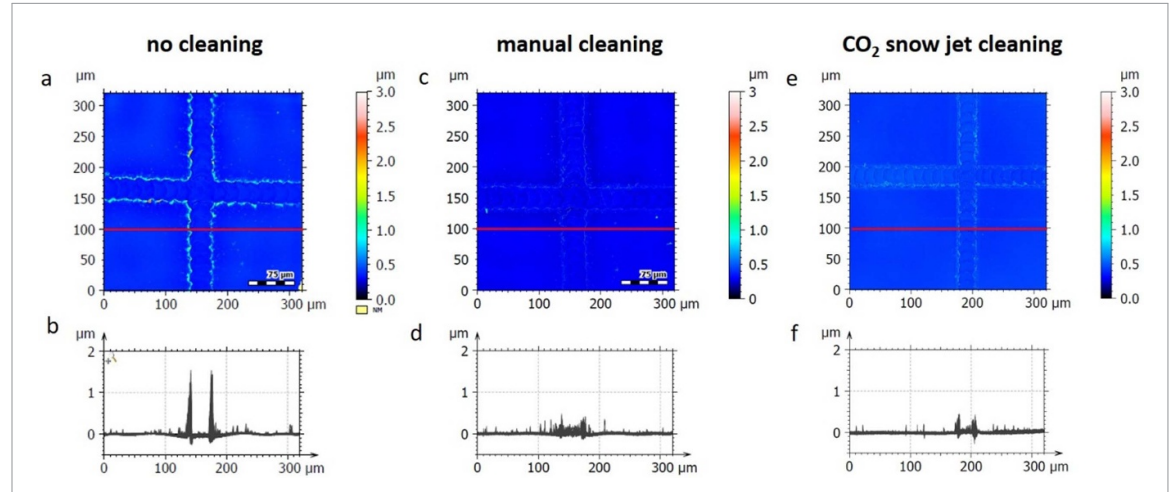


Figure 2. (a): Confocal microscope image of uncleaned P1 laser lines on an IMI substrate. (b): Height profile along the red line in figure (a) with laser-induced burrs visible at 135 and 175  $\mu$ m. (c): Confocal microscope image of manually cleaned P1 laser lines on an IMI substrate. (d): Height profile along the red line in figure (c). (e): Confocal microscope of P1 laser lines on an IMI substrate, cleaned by CO<sub>2</sub> snow jet. (f): Height profile along the red line in figure (e).

Module fabrication requires the three patterning steps P1, P2, and P3, which correspond to the partial ablation of bottom electrode, active layers, and top electrode, respectively (figure 1(a)). In industrial R2R production, sandwich structures of ITO (40 nm)/Ag (10 nm)/ITO (40 nm) sputtered onto heat stabilized poly(ethyleneterephthalate) (PET) films are employed as transparent bottom electrodes almost exclusively, as they provide higher conductivity and superior flexibility than substrates with pure ITO [15, 16].

However, due to the very nature of the ITO/metal/ITO (IMI) sandwich structure of the transparent electrode, laser patterning (as well as other conceivable patterning methods, such as scratching) results in burring of the IMI coating at the edges of

the patterning lines [10, 13] with individual spikes protruding up to a few micrometers from the surface, but still being physically and electrically connected to the substrate (figures 1(a) and 2(a), (b)).

Since the active (i.e. photocurrent generating) layers in organic and perovskite solar modules are very thin, typically less than 500 nm, these conductive burrs come into contact with the top electrode in the finished module, thereby short-circuiting the module, thus causing substantial losses in FF and open-circuit voltage ( $V_{\rm OC}$ ). This leads to low production yields with many shorted modules and drastic performance degradation of the remaining functional devices. Making the active layer thicker alleviates the problem, but requires layer thicknesses of several hundred nanometers, which compromises

device performance and only reduces shunting rather than eliminating it. Attempts to avoid burring by varying laser parameters, including beam shaping, have not been successful. Thus, the removal of the burrs can currently only be achieved by 'shunt burning', i.e. applying a high reverse bias to finished modules, which leads to thermal elimination of the burrinduced shunts. However, this method only works for minor degrees of shunting, while shunt-burning of shunts, which seriously affect device performance, results in the complete failure of the module and therefore significantly reduces the yield of the produced modules. Thus, only the removal or reduction of the conductive spikes prior to application of the active layer has emerged as a sustainable method in the production of flexible solar modules.

The state of the art in this case is to remove or reduce the protruding spikes along the P1 lines on the laser-patterned IMI electrode with special solvent-soaked microfiber cloths by mechanical wiping by skilled technical staff (figures 2(c) and (d)). However, the success of this process is highly dependent on the care of the operator, since the IMI electrode is only 90 nm thick and can therefore be easily damaged between the patterning lines. If during cleaning the pressure of the tissue is too high, or unevenly applied, the IMI substrate will be scratched and the active area of the module is reduced (figure S1). If the cleaning is too weak, the burrs remain, causing localized shunts, which can create defects in the modules during operation or measurement (figure S2).

Obviously, this method is not compatible with industrial high-throughput processes. Attempts to industrialize this process have failed, as both, maintaining constant pressure over a large area on the moving film and continuously replacing used wipes have proven problematic. We have therefore attempted to develop a more appropriate method.

CO<sub>2</sub> snow jet cleaning has already found applications in the automotive and semiconductor industries as a cost-effective and gentle method for highthroughput deburring [17, 18]. When liquid CO<sub>2</sub> under pressure is vented, it freezes into microscopic snow-like crystals which can be blasted onto the surface with a supersonic jacket of compressed air (see figure 1(b)). Four effects contribute to the cleaning process, namely momentum transmission, rapid cooling, micro explosion and solvent effect. Momentum transmission from the CO<sub>2</sub> crystals to particles and microscopic burrs creates a force larger than the adhesive force of the contaminations, which are consequently removed. The dry ice crystals inside this jet have a temperature of -78.5 °C, which causes rapid cooling at the surface and immediately embrittles molecular contaminates, breaking them up into particles. Instantly, CO<sub>2</sub> sublimation takes place as the crystals turn to gas, expanding in volume by 600 times, causing micro explosions that dislodge the particles. Momentarily at impact, the snow crystals are compressed and reach a supercritical fluid phase, giving a solvent effect that helps to further rinse organic contaminates from the surface.

Deburring by CO<sub>2</sub> snow jet blasting has the advantage of applying a constant pressure with a strong horizontal component very homogeneously, which will allow the removal of spikes without damaging the IMI bottom electrode. In the following, we will thus describe the development of an industrially compatible CO2 snow-jet cleaning system (figure 1(c)) for the efficient elimination of burrs along the P1 laser patterning lines of IMI electrodes in organic photovoltaic modules. The implementation and integration of a fully automated CO<sub>2</sub> snow jet cleaning process into a R2R production line for printed photovoltaics opens the possibility to replace nonindustrial methods in established high-throughput processes, which will give a significant boost to the competitiveness of printed photovoltaics.

#### 2. Experimental

#### 2.1. Materials

The substrates utilized in this work are based on heat-stabilized PET (DuPont Teijin Films, Melinex® ST504) with transparent conductive coating of ITO (40 nm)-Ag (10 nm)-ITO (40 nm) (IMI) and were purchased from OPVIUS GmbH. The active materials poly(3-hexylthiophene) (P3HT) and (5Z,5'Z)-5,5'-((7,7'-4,4,9,9-tetraoctyl-4, 9-dihydro-s-indaceno[1,2-b:5,6-b']dithiophene-2,7-diyl)bis(benzo[c][1,2,5]thiadiazole-7,4-diyl))bis (methanylylidene bis(3-ethyl-2-thioxothiazolidin-4one)) (O-IDTBR) were purchased from OPVIUS and Nano-C, respectively. The solvents used to dissolve the active layer materials were o-xylene (o-XY, Sigma-Aldrich) and 1-methylnaphthalene (1-MN, Merck). The interlayers, tin oxide (SnO<sub>2</sub>, N31) and poly(3,4ethylenedioxythiophene)-poly(styrenesulfonate) (PEDOT:PSS) (HTL Solar) were purchased from Avantama AG and Heraeus, respectively. Finally, water-based silver nanowire (AgNW) ink, including nanowires with 25 nm diameter, was purchased from Zhejiang Kechuang Advanced Materials Technology Co., Ltd.

#### 2.2. R2R coating machine

The R2R coating machine consists of three slot die coating stations. Two of the coating stations are equipped with 2 m long hot air ovens for annealing of the layers deposited, while the third station, which is used for the coating of the semiconductor layer, has a heating mat installed directly after the coating unit. Additionally, air blades and a Teknek cleaning roller are included in the machine to get rid of any remaining loose particles on the substrate.

#### 2.3. R2R CO<sub>2</sub> cleaning machine

Three CO2 snow jet nozzles from acp Systems AG were installed on the R2R coating machine. The nozzles can be changed in height and angle to find the perfect parameter set of pressure of compressed air, speed of the machine and nozzle diameter, see figure 1(c).

#### 2.4. Fabrication of devices

The fabrication of the devices consists of six steps.

First step: R2R laser ablation of the P1 line on an 8 m long IMI roll, with an active area of 50 cm<sup>2</sup> for each module.

Second step: Cleaning of the substrate. One third of the roll was cleaned by CO<sub>2</sub> on a separate R2R machine (see next paragraph for details). The second third was manually cleaned with the commonly used method of manually wiping with a solvent-soaked antistatic fiber cloth and the third was not cleaned at all.

Third step: At a web speed of  $0.5 \text{ m min}^{-1}$ , the laser-patterned roll was then treated with compressed air by an air knife and superficially cleaned with a Teknek roller, for removing dust from the substrate. In the same process step, the SnO<sub>2</sub> electron extraction layer is coated with a slot die at a calculated dry film thickness of 20 nm and subsequently annealed inline for 4 min and 130 °C. P3HT:o-IDTBR is coated with a calculated dry film thickness of 230 nm, and dried for 1 min at 85 °C. PEDOT:PSS was coated, with a calculated dry film thickness of 75 nm. Fourth step: After the deposition of the first three layers, P2 was R2R laser patterned. Fifth step: AgNW were slot die coated at 1 m min<sup>-1</sup> with a resulting sheet resistance of approx. 8 Ohm sq<sup>-1</sup> and annealed for 2 min and 130 °C. Sixth step: P3 R2R laser patterning. The finished modules were separated and bus bars were applied for contacting.

#### 2.5. CO<sub>2</sub> snow jet cleaning

The cleaning tool was provided by acp systems. It consists of a media supply unit, which delivers filtered, chilled liquid CO<sub>2</sub> at 60 bars and compressed dry air at stable conditions, and up to three nozzles. The nozzles each consist of a fixed, annular de Laval geometry for accelerating the compressed air jacket to supersonic speed, and an exchangeable capillary in the center. By choking the internal flow, the capillary diameter determines the flow rate of CO<sub>2</sub> and the size of snow crystals formed. Diameters from 200  $\mu$ m to 400  $\mu$ m are available in 50  $\mu$ m steps. The small sizes are usually used for cleaning sensitive surfaces like imager chips or coated optics, whereas the larger diameters are used to remove more persistent contaminations or burrs. The compressed air pressure determines the momentum of the CO2 snow crystals and can be varied from 2 bars to 15 bars. The optimal distance from the nozzle to the surface varies between 35 mm and 100 mm, depending on pressure and capillary size, however, there is no sharp optimum which makes the distance a less sensitive parameter. The cleaning effect is maximum at perpendicular impact of the jet. By reducing the impact angle, the cleaning spot turns from circular to elliptical, hence beneficially increasing the working width at the cost of reduced cleaning effect.

#### 2.6. Characterization

The current density vs. bias (JV) characteristics of the solar modules are measured by using a source measure unit (Keysight B2901A, Keysight Technologies), a class AAA solar simulator (LOT Quantum Design) providing AM 1.5 G illumination of 1000 W cm<sup>-2</sup> and a special measurement board, which can be filled with nitrogen.

Dark lock-in thermography (DLIT) characterization was performed in a dark chamber with a Taurus  $10\,\mathrm{k}$  SM Pro IR camera from IRCAM GmbH to measure shunts (localized shorts) a reverse bias of  $-10\,\mathrm{V}$  was applied to the modules in the dark and the heat dissipated by the resulting currents is detected by the infrared camera. The voltage and the camera signal were pulsed at 50 Hz and 100 frames were integrated to obtain an image.

Microscopy: for imaging of the burrs the confocal microscope  $\mu$ surf from NanoFocus AG was used.

#### 3. Results and discussion

#### 3.1. R2R snow jet cleaning

For R2R cleaning of laser-patterned substrates for PV module production, the full width of the web must be reliably cleaned from burrs. For this purpose, we have set up a R2R pilot line system for large area deburring, which consists of an array of  $CO_2$  snow jet nozzles over the moving PET/IMI web (see figure 1(c)).

In the first step, the  $CO_2$  snow jet blasting parameters of a single nozzle were optimized, with the goal of obtaining a substantial decrease in burr height without damaging the surrounding IMI electrode. The parameters to be controlled are the capillary diameter of the nozzle, which controls the  $CO_2$  flow rate, compressed air jacket pressure, the speed of the web movement, the distance between nozzle and substrate and the inclination of the nozzles with respect to the substrate plane.

For this purpose, a test structure of parallel P1 laser lines running in machine direction, separated by 0.6 cm in transverse direction, was lasered on a 10 m long PET/IMI roll (see inset of figure 3(a)). The CO<sub>2</sub> nozzle was aligned directly at the center of the web and the cleaning process was started. After the cleaning procedure, the maximum peak heights of the burrs for each laser line were determined by means of confocal microscopy measurements and plotted vs. the distance of the respective laser line from the nozzle position. This procedure was performed for a multitude of cleaning parameter combinations. Parameters

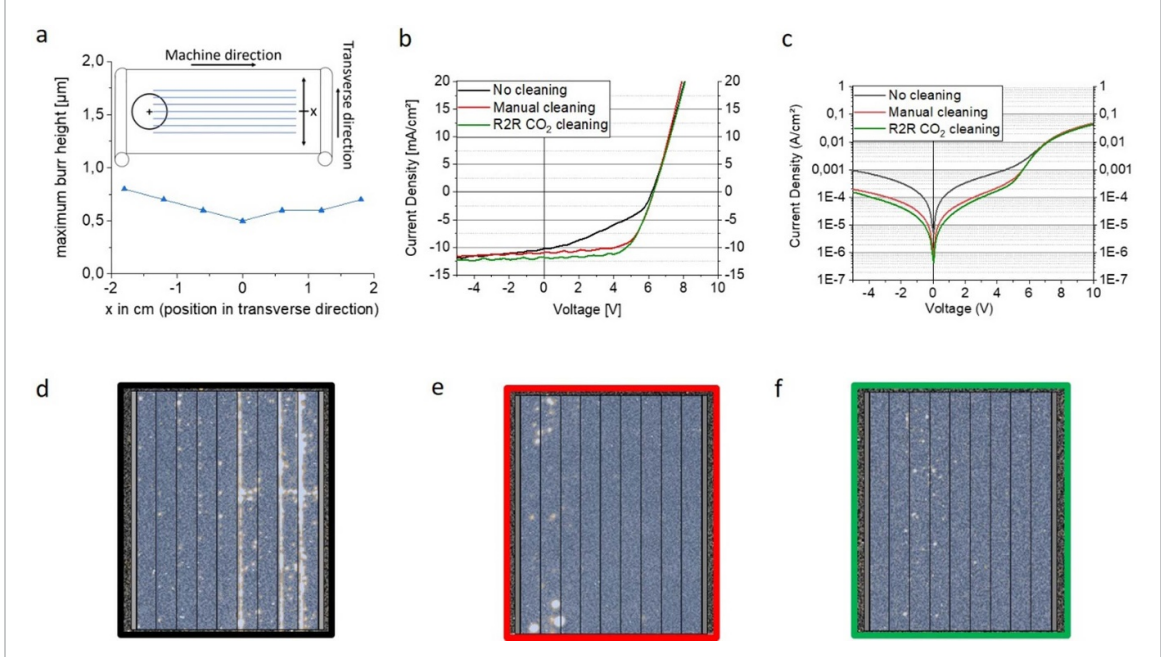


**Figure 3.** (a): Maximum peak height of the burrs versus the distance from the center of cleaning. A sketch of the test structure on the IMI roll with the nozzle center marked with a circle is shown in the inset. Light (b) and dark (c) current density-voltage characteristics of modules with uncleaned P1 line (black), hand cleaned P1 line (red) and roll-to-roll  $CO_2$  jet cleaned P1 line (green). DLIT images at reverse bias of -10 V, with photograph of module overlaid (blue: cells connected in series, grey: bus bar). (d): Uncleaned P1 line, (e): manually cleaned P1 line, (f): R2R  $CO_2$  cleaned P1 line.

varied were nozzle diameter (which determines the CO<sub>2</sub> flux), distance of nozzle to web, air pressure, inclination angle of nozzle, and web speed (figure S3 and table S1). Although the process window with respect to all of these parameters turns out to be conveniently wide, there is a clear tradeoff between CO<sub>2</sub> flux and air pressure on one hand and distance between nozzle and web on the other hand. Satisfactory deburring is obtained for nozzle diameters above 300  $\mu$ m. Air pressure must be at least 3 bars, as for lower values the CO<sub>2</sub> jet quality deteriorates noticeably. On the other hand, if air pressure significantly exceeds 3 bars, damage of the IMI layer is observed. However, this occurs only for the combination of large nozzle diameters of 400  $\mu$ m and close distances of the nozzle to the web, in the range of few centimeters. For medium nozzle diameters of 350  $\mu$ m the distance to the web can be varied over a wide range of 1.5-13 cm. Larger distances result in slightly larger cleaning diameters, but if the distance is too large, the burrs are not removed reliably. Web speed has very little effect on deburring quality. Actually, in the range of web speeds usually employed for printing OPV modules, i.e. 0.5-3 m min<sup>-1</sup>, no dependence was observed at all.

The best cleaning result yields burr heights of less than 800 nm over an effective cleaning width of  $\sim$ 4 cm (figure 3(a)) and is obtained for the following parameter set:

- (a) Nozzle inclination: 60°.
- (b) Nozzle-to-substrate distance: 13 cm.
- (c) Web speed:  $1 \text{ m min}^{-1}$ .

- (d) Capillary size: 350  $\mu$ m.
- (e) Air pressure: 3 bar.
- (f)  $CO_2$  flow: 0.18 l min<sup>-1</sup>.

The confocal microscope image and the corresponding height profile of the P1 line at the nozzle position (x = 0) for the best parameter set are shown in figures 2(e) and (f).

In the following, for the cleaning of solar modules of 8 cm in width, an array of three snow jet nozzles at a distance of 3 cm is used, which results in an overlap of the effective cleaning widths of the individual nozzles, and thus provides a gapless and reliable cleaning of the whole substrate.

### 3.2. Module manufacturing on CO<sub>2</sub> snow jet treated substrates

In order to evaluate the effect of deburring on photovoltaic performance, OPV modules were manufactured on the CO<sub>2</sub> snow jet treated substrates and compared to those manufactured on pristine and manually cleaned ones. All layers where R2R slot die coated on laser-patterned IMI rolls with these three different variations: uncleaned, manually cleaned and R2R CO<sub>2</sub> snow jet cleaned. In figures 3(b) and (c), representative light and dark JV curves of modules of these three variations are shown. The respective photovoltaic key parameters are listed in table 1. As described previously, the modules on the uncleaned substrate suffer from a high leakage current, which significantly reduces the FF to 37% and in turn the photoelectrical conversion efficiency (PCE) to 2.3%. The modules on the manually cleaned substrate do not

**Table 1.** Photovoltaic key parameters, short circuit current  $(I_{sc})$ , open circuit voltage  $(V_{oc})$ , fill factor (FF), and photoelectric conversion efficiency (PCE) (average values of five modules per variation, values of the best performing modules are shown in bold).

Variation	Isc (mA)	Voc (V)	FF (%)	PCE (%) active area	PCE (%) total area	Number of cells in series	Active area per cell (cm <sup>2</sup> )	Module area (cm²)
No cleaning	$42.78 \pm 4.95$	$6.24 \pm 0.04$	$36.72 \pm 1.66$	$2.27 \pm 0.27$	$2.05 \pm 0.24$	9	4.8	47.6
	49.40	6.19	37.37	2.6	2.40			
Hand cleaning	$51.97 \pm 0.80$	$6.29 \pm 0.01$	$63.92 \pm 0.53$	$4.83 \pm 0.06$	$4.38 \pm 0.06$			
	52.54	6.29	64.15	4.91	4.44			
R2R CO <sub>2</sub>	$56.04 \pm 0.72$	$6.31 \pm 0.02$	$64.88 \pm 0.49$	$5.31 \pm 0.07$	$4.81 \pm 0.06$			
cleaning	56.87	6.33	65.39	5.45	4.94			

exhibit such shunting issues and possess the expected photovoltaic performance with PCE values of 4.8% (with respect to the active area). The modules on the  $\mathrm{CO}_2$  snow jet cleaned substrates also do not show any sign of shunting and, remarkably, have even higher PCEs (5.3%) than the manually cleaned ones, which is mainly due to a superior short-circuit current ( $J_{\mathrm{SC}}$ ). This may be explained by the fact that manual cleaning always leads to a certain extent of scratching of the IMI electrode, which can reduce the active area significantly, since not only the area of a scratch itself does not generate photocurrent, but also areas (that have still intact IMI), which are cut off from the point of charge extraction by a scratch do not contribute to  $J_{\mathrm{sc}}$ .

To confirm that the difference in performance of differently treated substrates is due to deburring, DLIT measurements were performed. The module on an uncleaned substrate shows brightly illuminated interconnection zones, which indicates a high density of shunts (see figure 3(d)). These shunts are predominantly located on the right side of the dark (inactive) area, which is defined by the P3 line on the left and the P1 line on the right. Consequently, the shunts are indeed caused by the burrs along the P1 lines. For the other two variations, namely manually cleaned (figure 3(e)) and CO<sub>2</sub> snow jet cleaned ones (figure 3(f)), only a few defects inside the active area are visible. However, these defects obviously do not have a negative effect on the photovoltaic device performance at 1000 W m<sup>-2</sup>, in contrast to the aforementioned defects along the P1 lines for uncleaned substrates.

#### 4. Conclusion

Shunting by laser induced burrs in printed solar modules can be eliminated reliably **over large areas** by CO<sub>2</sub> snow blasting. In contrast to manual cleaning, which has been the standard method so far, CO<sub>2</sub> snow blasting is R2R compatible and thus enables high throughputs. On a prototype system, it has been verified for a 10 cm wide substrate and a web speed of 1 m min<sup>-1</sup>, that the burrs can be reliably removed and the solar modules thus produced do not show any short circuits, which significantly improves their performance.

#### Data availability statement

The data that support the findings of this study are available upon request from the authors.

#### Acknowledgments

Financial support by the German Ministry of Economy and Climate Protection in the framework of the ZIM program is acknowledged (FKZ KK5094994GM1). H-J E, A D, H-D S, and C J B acknowledge the 'Solar Factory of the Future' as part of the Energy Campus Nuremberg (EnCN), which is supported by the Bavarian State Government (FKZ 20.2-3410.5-4-5). The authors also acknowledge funding from the European Union's Horizon 2020 research and innovation program under Grant Agreements No. 952911 ('BOOSTER') and 101007084 ('CITYSOLAR'). H-J E and C J B acknowledge funding from the European Union's Horizon 2020 INFRAIA program under Grant Agreement No. 101008701 ('EMERGE').

#### **ORCID** iDs

A Distler https://orcid.org/0000-0003-3500-2180 H-JHJ Egelhaaf https://orcid.org/0000-0002-8263-8125

#### References

- [1] NREL Best research-cell efficiency chart (available at: www. nrel.gov/pv/assets/pdfs/best-research-cell-efficienciesrev220630.pdf)
- [2] Zhu L et al 2022 Single-junction organic solar cells with over 19% efficiency enabled by a refined double-fibril network morphology Nat. Mater. 21 656–63
- [3] Zhao Y, Zhang J, Xu Z, Sun S, Langner S, Hartono N T P and Brabec C J 2021 Discovery of temperature-induced stability reversal in perovskites using high-throughput robotic learning Nat. Commun. 12 1–9
- [4] Green M A, Dunlop E D, Hohl-Ebinger J, Yoshita M, Kopidakis N, Bothe K, Hinken D, Rauer M and Hao X 2022 Solar cell efficiency tables (Version 60) *Prog. Photovolt., Res.* Appl. 30 687–701
- [5] NREL Best champion-module efficiency chart (available at: www.nrel.gov/pv/assets/pdfs/champion-module-efficienciesrev220401b.pdf)
- [6] Distler A, Brabec C J and Egelhaaf H-J 2021 Organic photovoltaic modules with new world record efficiencies *Prog. Photovolt.*, Res. Appl. 29 24–31

- [7] Pescetelli S, Agresti A, Viskadouros G, Razza S, Rogdakis K, Kalogerakis I and Di Carlo A 2022 Integration of two-dimensional materials-based perovskite solar panels into a stand-alone solar farm *Nat. Energy* 7 597–607
- [8] Reddy S H, Di Giacomo F and Di Carlo A 2022 Low-temperature-processed stable perovskite solar cells and modules: a comprehensive review Adv. Energy Mater. 12 2103534
- [9] Yang F, Jang D J, Dong L R, Qiu S, Distler A, Li N, Brabec C J and Egelhaaf H-J 2021 Upscaling solution-processed perovskite photovoltaics Adv. Energy Mater. 11 2101973
- [10] Lucera L, Kubis P, Fecher F W, Bronnbauer C, Turbiez M, Forberich K, Ameri T, Egelhaaf H-J and Brabec C J 2015 Guidelines for closing the efficiency gap between hero solar cells and roll-to-roll printed modules *Energy Technol*. 3 373–84
- [11] Lucera L, Machui F, Kubis P, Schmidt H D, Adams J, Strohm S, Ahmad T, Forberich K, Egelhaaf H-J and Brabec C J 2016 Highly efficient, large area, roll coated flexible and rigid OPV modules with geometric fill factors up to 98.5% processed with commercially available materials Energy Environ. Sci. 9 89–94

- [12] Kubis P et al 2014 High precision processing of flexible P3HT/PCBM modules with geometric fill factor over 95% Org. Electron. 15 2256–63
- [13] Kubis P et al 2019 All sub-nanosecond laser monolithic interconnection of OPV modules Prog. Photovolt., Res. Appl. 27 479–90
- [14] Kubis P, Li N, Stubhan T, Machui F, Matt G J, Voigt M M and Brabec C J 2015 Patterning of organic photovoltaic modules by ultrafast laser *Prog. Photovolt.*, Res. Appl. 23 238–46
- [15] Ferhati H, Djeffal F and Benhaya A 2019 Optimized high-performance ITO/Ag/ITO multilayer transparent electrode deposited by RF magnetron sputtering Superlattices Microstruct. 129 176–84
- [16] Guillén C and Herrero J 2008 ITO/metal/ITO multilayer structures based on Ag and Cu metal films for high-performance transparent electrodes Sol. Energy Mater. Sol. Cells 92 938–41
- [17] acp systems AG 2022 Automotive (available at: www.acpsystems.com/automotive/)
- [18] acp systems AG 2022 Medizintechnik (available at: www.acp-systems.com/medizintechnik/)